Comparison of Displacement and Gas Production Rates in Current Fission and Future Fusion Reactors

G.L. Kulcinski, D.G. Doran, and M.A. Abdou

May 1972
(revised April 1974)

UWFDM-15

FUSION TECHNOLOGY INSTITUTE

UNIVERSITY OF WISCONSIN

MADISON WISCONSIN

Comparison of Displacement and Gas Production Rates in Current Fission and Future Fusion Reactors

G.L. Kulcinski, D.G. Doran, and M.A. Abdou

Fusion Technology Institute
University of Wisconsin
1500 Engineering Drive
Madison, WI 53706

http://fti.neep.wisc.edu

May 1972 (revised April 1974)

UWFDM-15

Comparison of Displacement and Gas Production Rates in Current Fission and Future Fusion Reactors

by

G. L. Kulcinski
*D. G. Doran
M. A. Abdou

April 8, 1974

*Hanford Engineering Development Laboratory, Richland, Washington

Abstract

The displacement, helium production and hydrogen production rates in 5 candidate materials for controlled thermonuclear reactors (316 stainless steel, Mo, Nb, V and sintered aluminum product) were calculated for seven potential irradiation facilities. The damage rates were calculated for two fast fission reactors (FFTF and EBR-II), two thermal reactors (HFIR and ETR), two accelerator neutron sources (LAMPF and RTNS), and a typical CTR blanket. It was found that while fission reactors can easily duplicate displacement damage rates typical of CTR first walls, they fall short, sometimes by several orders of magnitude, of duplicating the helium and hydrogen production rates. The one exception to the latter statement is that helium production in stainless steel, due to the ^{59}Ni production, can even be higher in thermal fission reactors than in CTRs. Accelerator sources produce damage which is more like that in CTRs, but the absolute magnitude in current facilities is too low by at least an order of magnitude. It is concluded that HFIR is the best current neutron facility to simulate fusion reactor damage.

I. Introduction

The structural components of controlled thermonuclear fusion reactor (CTR) blankets will be subjected to the most severe high temperature irradiation environment that has ever been imposed on solid materials.[1-5] The safe and economical operation of CTRs will, to a large degree, depend on how successful scientists are in choosing metals and alloys that can retain adequate strength, ductility, and dimensional stability under such conditions. These mechanical and physical properties are very sensitive to the total number of times each atom is displaced in a solid during the component's lifetime.[6-9] Previous estimates[1-5] predicted that the atoms in CTR blanket components will theoretically be displaced up to several hundred times per year at temperatures of 500-1000°C. These displaced atoms and their vacant lattice sites are known to precipitate into clusters which can cause significant volume changes.[6-8] Another factor which has been shown to greatly effect the mechanical properties of metals irradiated in fission reactors is the amount of neutronically generated gases present in metal. These gases come from (n,α), (n,n'α), (n,p), (n,n'p), (n,d), and (n,t) reactions characteristic of high energy neutrons. The cross sections for such reactions are usually appreciable only above a few MeV in most elements. Whereas it has already been found that helium concentrations typical of fission reactor environments (~1-10 atomic ppm) can cause high temperature embrittlement,[9-11] the situation is expected to be much worse for CTRs because the transmutation cross sections for the 14 MeV neutrons are much higher.

It is obvious that if we ever expect to construct large scale CTRs, we must know the quantitative values of the displacement and transmutation

rates in potential CTR materials. Since high power fusion reactors won't be available until the late 1980's[12], we must also attempt to simulate those conditions as best we can in current irradiation facilities and test the components under typical CTR conditions to see if they will meet the design requirements.

The main purpose of this paper is to show what range of displacement and transmutation rates we might expect in fusion reactors for materials such as Nb, V, Mo, Al or stainless steel, which are currently being considered for CTR applications. We will also address the question of what current facilities (fast and thermal reactors as well as 14 MeV accelerator neutron sources) might be used to simulate the calculated damage rates.

We must limit our discussion, as in most exercises of this type, to our current concept of how a CTR blanket might look some 20 years from now. Therefore, we have chosen a blanket similar to that designed by the University of Wisconsin Fusion Reactor Study Group.[13] It is felt that this blanket is a reasonable structure to accomplish the neutron slowing down, energy removal, and breeding objectives of a CTR. We recognize that the ultimate blanket design will be much more detailed and perhaps somewhat different in its size, shape and placement of major components.

II. Description of Calculational Procedures

A. Blanket Design

The CTR blanket design chosen for this study is shown schematically in Figure 1 and is similar to that used for a 5000 MW_{th} Tokamak reactor.[13] The details of the structure have been homogenized in a manner better suited for neutronics calculations. There are basically five regions to consider: a 1 cm thick first wall, a 42 cm thick breeding and cooling zone which is 95% natural lithium and 5% structural material, a 20 cm thick stainless steel

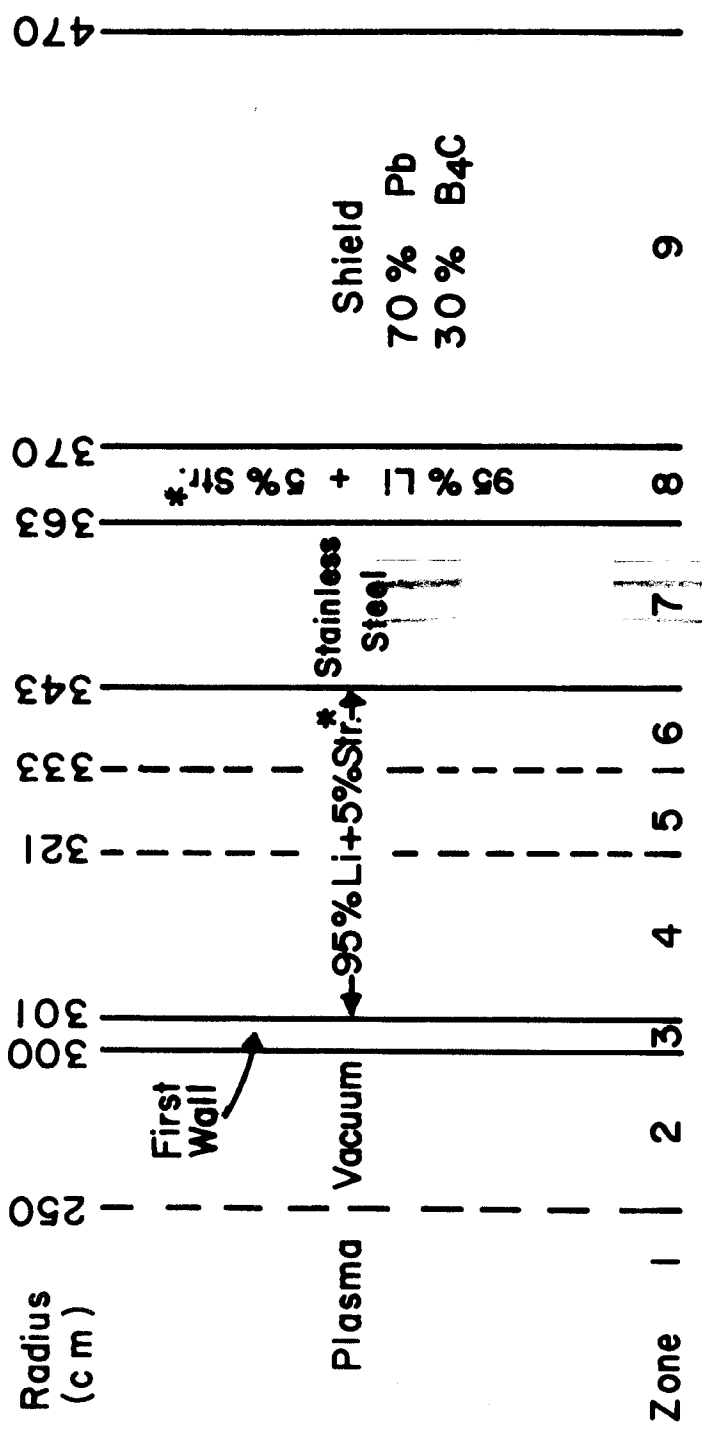

Fig. 1 CTR Blanket Design used for comparison of gas production And displacement rates.

reflector, a 7 cm thick cooling region again composed of 95% Li and 5% structure, and a one meter thick shield composed of 70% Pb and 30% B_4C.

B. Flux Spectra

The neutron spectra in the various blankets have been calculated by substituting the various metals into the fusion blanket described previously and using the discrete ordinate program ANISN.[14] All calculations were made in one-dimensional cylindrical geometry using the P_3-S_6 approximations. Neutron cross section data has been obtained from ENDF/B-III[15] and processed by MACK[16] into either a 100 or 46 energy group structure ranging from 0.022 eV to 14.918 MeV. The 14 MeV neutron source to the first wall was normalized to 1 MW/m^2 ($4.43 \times 10^{13} n/cm^2/sec$) so that all CTR results are reported per unit of neutron wall loading.

The same volume of metal was used in each fusion blanket calculation although in practice the amount may vary with the specific material (e.g., less Mo may be needed than Al). However, since the spectra in a fusion reactor are primarily determined by the lithium, the exact amount of structural material has very little effect on the neutron spectra. It should be noted that it is not practical to consider pure Al as a wall material because of its low strength at high temperature. Therefore, we have used Sintered Aluminum Product (SAP) as a realistic substitute. SAP is simply high purity Al which is strengthened by the addition of 5-10% by weight of Al_2O_3 in the form of very fine particles in the matrix. Some characteristics of this material for CTR application have recently been described by Powell et.al.[17]

The neutron flux spectra for two fast reactors, EBR-II and FFTF were obtained from the Dosimetry Center, Hanford Engineering Development

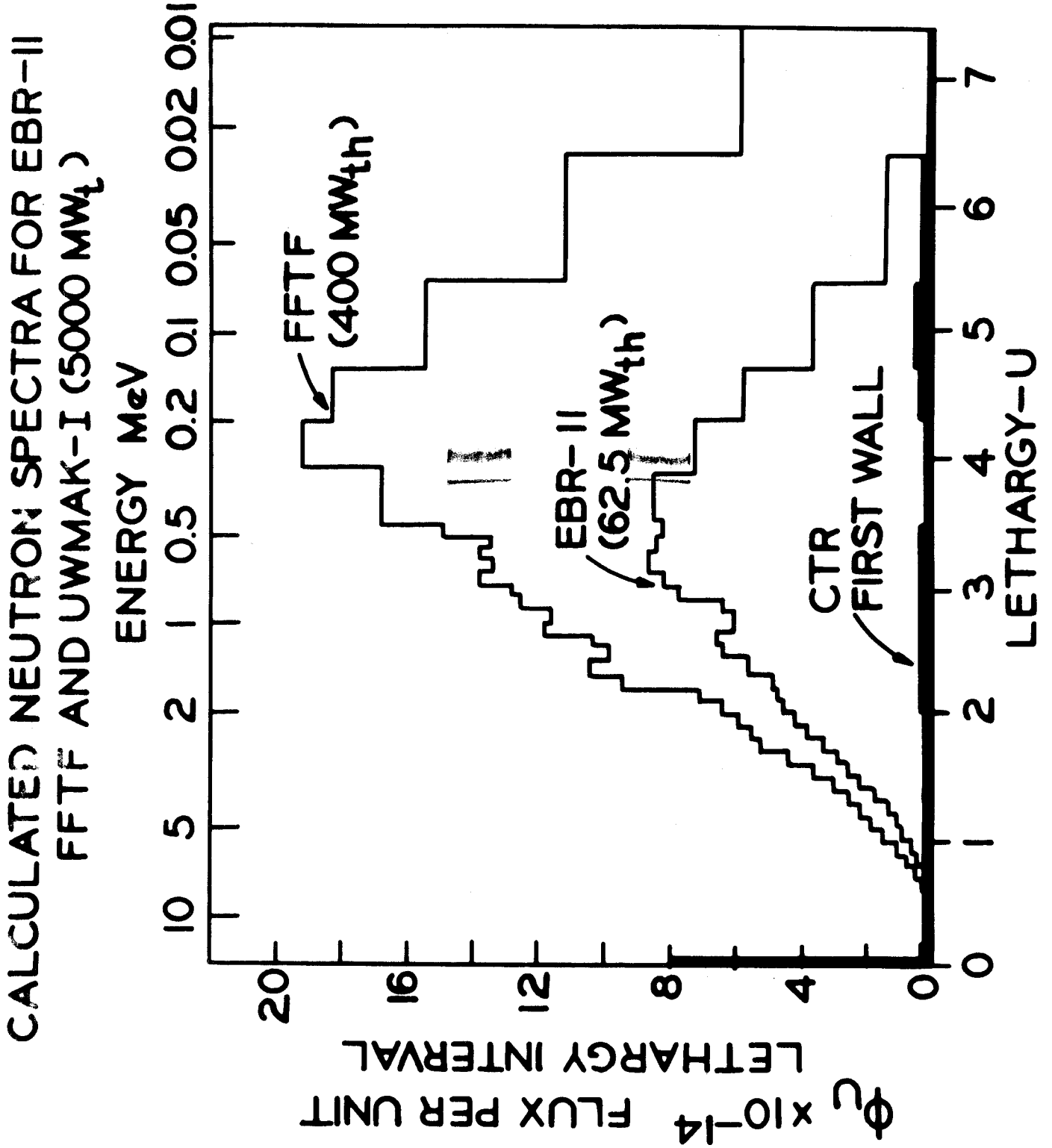
CALCULATED NEUTRON SPECTRA FOR EBR-II
FFTF AND UWMAK-I (5000 MWt)
ENERGY MeV
10 5 2 1 0.5 0.2 0.1 0.05 0.02 0.01
FFTF
(400 MWth)
EBR-II
(62.5 MWth)
CTR
FIRST WALL
20 16 12 8 4 0
$\phi_u \times 10^{-14}$ FLUX PER UNIT
LETHARGY INTERVAL
0 1 2 3 4 5 6 7
LETHARGY-U

FIG. 2

Laboratory. The core center, row two spectra at 62.5 MW(th) as unfolded by SAND-II was used for EBR-II and the core center driver fuel assembly spectrum was used for FFTF. Data from two current thermal test reactors, ETR and HFIR[18], were also used. The target spectrum in HFIR, PTP location, was used for 100 MW operation and the midplane data for row L-8 unfolded by SAND-II were used for ETR operating at 175 MW. A comparison of the neutron spectra for the two fast reactors to that calculated for a 316 SS CTR blanket wall is shown in Figure 2. Note the relatively low neutron fluxes in the CTR for the region below 5 MeV and the large peak in the CTR spectrum at 14 MeV.

The neutron spectra for the LAMPF facility were obtained from Dudziak and Sherman[19] for a 0.5 mA beam of 800 MeV protons on a water cooled copper target with a nickel reflector. The total flux at the sample was calculated to be 2×10^{14} n/cm^{2}sec of which only 3.36% is above 10 MeV and 1.45% in the 10-25 MeV interval.

The rotating target neutron source (RTNS) at Lawrence Livermore Laboratory[20] currently has a 14 MeV current of $\sim 2 \times 10^{12}$ n/cm^{2}sec. At the present time there is no provision for surrounding samples with CTR type blankets to take advantage of backscattered neutrons, although such a facility would be relatively easy to build. Therefore, we have assumed the theoretical displacement and gas production rates in the RTNS would be similar to those in a CTR first wall but scaled down to a 0.045 MW/m^2 wall loading.

C. Displacement Cross Sections

Neutron interactions with nuclei that are treated explicitly in this work include elastic scattering, inelastic scattering, (n,2n) and (n,γ). Charged particle reactions are neglected for all metals but aluminum. This introduces

no more than a 5% error in the displacement cross sections of the refractory metals and 15% in stainless steel at 15 MeV. The error decreases rapidly with decreasing energy. In the case of aluminum, (n,α) and (n,p) reactions are included in an approximate manner by adding the cross sections to the inelastic scattering cross section. This is to take account of the kinetic energy given the emitting nucleus. The damage produced by the emitted proton or alpha particle is negligible; e.g., the number of displacements produced by the alpha particle in the $^{27}Al(n,\alpha)^{24}Na$ reaction was estimated to be <1% of that produced by the nucleus. The charged particle reactions add ~30% to the displacement cross section of Al at 15 MeV.

It should be pointed out that charged particle reactions, including (n,np), dominate the displacement cross section of Ni at 15 MeV and should be taken into account in any consideration of high Ni content alloys.

The mechanisms listed above produce primary knock-on atoms (PKAs) which in turn lose their energy by electronic excitation or nuclear energy transfers to surrounding atoms. This latter form of energy transfer causes further displacements. The total displacement cross section at energy E is just

$$F(E) = F_{el}(E) + F_{inel}(E) + F_{(n,2n)}(E) + F_{(n,\gamma)}(E) \qquad (1)$$

where $F_{el}(E)$ is the displacement cross section due to both isotropic scattering at low energies (<0.1 MeV) and anisotropic scattering at higher energies

$F_{inel}(E)$ is the displacement cross section due to (n,n') scattering.

$F_{(n,2n)}(E)$ is the displacement cross section due to (n,2n) reactions.

$F_{(n,\gamma)}(E)$ is the displacement cross section due to the energetic recoils which result from (n,γ) reaction (mainly from low energy neutrons).

The general expression for F(E) is

$$F(E) = \sigma(E) \int_{E_d}^{T_{max}} p(\bar{E},T)\ \nu(T)dT \qquad (2)$$

where $\sigma(E)$ is the appropriate interaction cross section.

$p(E,T)$ is the probability that a neutron of energy E transfers T to the PKA.

$\nu(T)$ is the number of displacements produced by a PKA with energy T.

and E_d is the minimum energy required to displace an atom.

The problem then boils down to a determination of the number and energy spectrum of the PKAs from $\sigma(E)$ and $p(E,T)$, and the choice of a model to calculate the average number of atoms displaced by each PKA of energy T. The evaluation of $\nu(T)$ is essentially independent of the type of scattering that produced the PKA and we will consider this problem first.

The results for this study are based on the Lindhard[21] theory of slowing down of energetic atoms in solids. Lindhard has derived, from Thomas-Fermi theory, a function $L(\varepsilon)$ which is the kinetic energy (in dimensionless form) that is transferred to the atoms of a cascade initiated by a PKA having initial dimensionless energy ε. That is, the fraction of PKA energy available to cause displacements is $L(\varepsilon)/\varepsilon$; the remainder is lost in electron excitation. In the present work, the number of displacements per PKA is calculated to be,

$$\nu(T) = \beta \frac{L(\varepsilon)}{\varepsilon} \frac{T}{2E_d} \ . \qquad (3)$$

where E_d is the effective displacement energy,

$\varepsilon = A_L T$ and for pure materials of atomic number Z and atomic weight A,

$$A_L = \frac{0.01151}{(Z)^{7/3}} \text{ eV}^{-1} .$$

$$L(\varepsilon) = \frac{\varepsilon}{[1+K_L g(\varepsilon)]} \qquad \text{(see Reference 22)}$$

where $g(\varepsilon) = \varepsilon + 0.40244\varepsilon^{3/4} + 3.4008\varepsilon^{1/6}$

and $K_L = \frac{0.1334(Z)^{2/3}}{A^{1/2}}$

$\beta \cong 0.8$

Beta is a numerical factor to account for the deviation from a hard sphere potential during a two body collision.[23]

It should be noted that $\nu(T)$ is very sensitive to the choice of E_d. There is considerable controversy over what one should use for this number; the threshold energy required to displace an atom in the easiest direction, or the maximum energy required to displace an atom in the close packed direction, or some arbitrary combination of all these values. Because of this uncertainity, we have chosen to report the displacement cross section in terms of barn-eV which will allow each investigator to choose his own value of E_d.

It has recently been suggested that the effective displacement energy in iron might be taken as 1.67 times the threshold value.[23] For lack of a more definite model at this time, we will use the same factor to multiply the threshold displacement energies of the materials considered here. The threshold energies used were, 36 eV for Nb[24], 37 eV for Mo[25], 24 eV for Fe[25], and 16 eV for Al[26]. We have arbitrarily chosen the threshold displacement energy as 24 eV for V in keeping with bcc Fe.*

*Note: The displacement energy of V has been recently measured to be 26eV (Miller and Chaplin, Radiation Effects, 22, 107, 1974)

The calculation of the PKA energy spectrum is rather straightforward in principle for elastic scattering and (n,γ) reactions but somewhat more complex for inelastic scattering and (n,2n) reactions. It is not the purpose of this paper to discuss the latter two scattering processes in detail as that is covered elsewhere.[27] Only the important points that pertain to this calculation will be presented here.

The principal source of cross section data for all metals but Fe was ENDF/B-III.[15] In the case of iron, MAT-1124 data were used. This evaluation differs insignificantly for the present application from the MAT-1180 evaluation included in ENDF/B-III. Some smoothing in the resonance region was carried out for V, Mo, Cr, and Ni, and some angular distribution data for Cr and Mo were taken from the third election of BNL-400.

The energy of the recoil atoms from (n,γ) reactions was taken as

$$T = \frac{[E_\gamma(\text{MeV})]^2}{1.862 \times 10^{-3}(A+1)} \qquad (4)$$

where the mean recoil energies were derived from a recent compilation of gamma ray spectra by Orphan et al.[28]

Both isotropic and anisotropic scattering was considered for the case of elastic collisions. In the isotropic region below E ≃ 0.1 MeV, the form of p(E,T) is just $(T_{max})^{-1}$ where $T_{max} = \gamma E$ and $\gamma = 1.009\ A/(1.009+A)^2$. At higher energies, available data in the ENDF

file on angular distributions permit the calculation of $p(E,T)$ from the expression $(2\pi/\sigma(E))\ (d\sigma(E,\mu)/d\Omega)$, where $\mu = \cos\phi$, ϕ = angle of scattering in the center of mass (CM) system, and Ω is unit of solid angle. The recoil energy T and μ are related through the expression

$$T = \frac{\gamma E}{2}(1-\mu).$$

For energies not greatly exceeding the inelastic scattering (n,n') threshold, the (n,n') contribution to the displacement cross section can be obtained as a sum of contributions from resolved energy levels Q_i (taken positive here). At higher neutron energies, the inelastic scattering is described by an evaporation model characterized by an effective evaporation temperature $\theta(E)$. In this model, the energy E_m, of the scattered neutron in the CM system is distributed as[27]

$$f(E,E_m) = \frac{E_m}{I(E,\theta)} \exp(-E_m/\theta) \qquad (5)$$

where $I(E,\theta) = \theta^2\{1-(1+E_m^{max}/\theta)\exp(-E_m^{max}/\theta)\}$

$$E_m^{max} = \eta_1(\eta_1 E - Q_1).$$

The value of Q_1 is the lowest resolved energy level and $\eta_1 = \frac{A}{1.009+A}$. The upper[(+)] and lower[(-)] limits of the recoil energy are now

$$T^{\pm} = \eta_1\eta_2 E + \frac{\eta_2}{\eta_1} \pm 2\eta_2(E\,E_m)^{1/2} \qquad (6)$$

where $\eta_2 = \frac{1.009}{1.009+A}$.

Finally, the (n,2n) contribution was based on a 2-n model with Odette's[29] modification of the sequential emission formulation of Segev[30]. A second neutron can be emitted only if the residual excitation of the nucleus after emission of the first neutron exceeds the binding energy U of a neutron in the mass A nuclide. The recoil energy after the emission of the first neutron was taken to be the average value $\bar{T}_1 = \eta_1\eta_2 E + \frac{\eta_2}{\eta_1} E_m$ and the total recoil energy after emission of a second neutron with E'_m is just

$$T = \left(\frac{A}{A-1}\right)\left(\frac{\eta_2}{\eta_1}\right)E'_m + \left(\frac{A-1}{A}\right)\bar{T}_1 - \frac{2(\eta_2)^{1/2}}{\eta_1}(\bar{T}_1 E'_m)^{1/2} + U. \qquad (7)$$

In summary, the form of F(E) used for the four cases of interest is given in Table 1 and the cross sections multiplied by displacement energies are compared in Figure 3 and listed in Table 2 (the unit is barn-eV). Displacement cross sections corresponding to different values of E_d than used here can be obtained by dividing the values in Table 2 by the preferred values of E_d. It should be realized, however, that this procedure is inaccurate when applied to the elastic scattering of neutrons in the few hundred to few thousand eV range. This is because the corresponding PKA energies are not sufficiently greater than E_d that the lower limit of the integral of equation (2) can be taken as 0. Hence, the displacement cross section is not strictly inversely proportional to E_d in this range.

TABLE 1

Summary of Various Displacement Cross Section Used for This Study

Method of Recoil Production	Form of F(E) - Displacement Cross Section per atom per unit of fluer
Elastic Scattering (isotropic & anisotropic)	$\sigma^{el}(E) \int_{-1}^{1-r} p(E,\mu)\nu[T(E,\mu)]d\mu$ $\quad r \equiv 2E_d/T_{max}$
Inelastic Scattering	
Resolved Energy Region	$\sum_i \sigma_i^{in}(E) \int_{-1}^{1} p_i(E,\mu)\nu[T(E,\mu)]d\mu$
Continuum	$\frac{\sigma^{in}(E)}{2} \int_0^{E_m^{max}(E)} \int_{-1}^{1} f(E,E_m)\nu[T(E,E_m,\mu)]d\mu dE_m$
(n,2n) reaction (a,b)	$\sigma^{n,2n}(E) \int_0^{E-U} \frac{E_m}{I(E)} \exp[-E_m/\theta(E)] \int_0^{E-U-E_m} \frac{E_m'}{I(E,E_m)} \exp[-E_m'/\theta(E)] \int_{-1}^{1} \frac{\nu}{2} [T(E,E_m,E_m',\mu)]d\mu dE_m' dE_m$
(n,γ) reaction	$\sigma^{(n,\gamma)}(E) \frac{[E_\gamma(MeV)]^2}{3.724\times10^{-3}(A+1)E_d}$

a) $I(E) = I(E,\theta)$ of Eq. 5 with $E_m^{max} = E-U$

b) $I(E,E_m) = I(E,\theta)$ of Eq. 5 with $E_m^{max} = E-U-E_m$

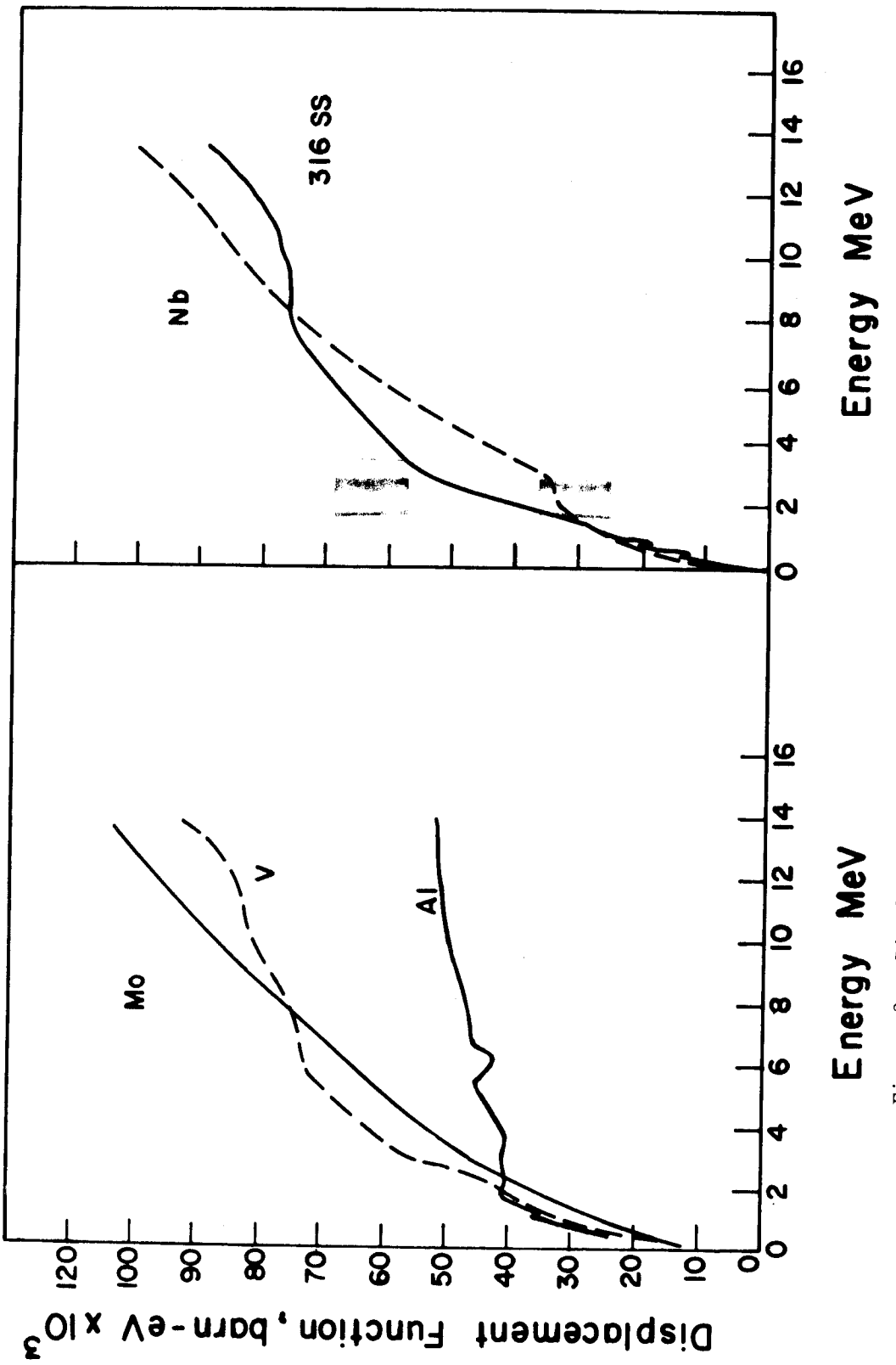

Figure 3. Displacement Function Values for Various CTR Materials

Table 1

Displacement Functions for Potential CTR Materials*

barn - eV

Lower Neutron Energy MeV	316 SS	Mo	Nb	V	Al
13.50	89,000	108,000	103,000	91,400	51,300
12.21	83,100	103,000	96,800	86,900	50,900
11.05	79,700	96,000	91,100	84,000	50,200
10.00	78,200	90,100	86,100	82,300	48,600
9.048	76,500	84,000	82,300	80,500	46,200
8.187	76,100	79,000	78,300	79,000	45,600
7.408	75,900	77,300	74,300	77,600	45,600
6.703	73,900	71,300	69,900	76,100	45,200
6.065	70,500	68,300	65,200	74,500	41,800
5.488	68,100	64,600	60,600	72,800	45,400
4.966	66,400	59,500	56,100	70,200	44,200
4.493	64,900	56,500	51,800	67,800	43,200
4.066	62,400	54,700	47,800	65,200	41,300
3.679	59,700	52,000	44,200	60,300	41,800
3.329	56,400	48,100	41,000	59,000	41,000
3.012	55,000	46,800	38,200	55,700	40,000
2.725	51,800	45,700	36,600	54,500	39,300
2.466	51,000	43,900	36,600	50,100	41,500
2.231	46,700	41,700	35,900	44,900	35,400
2.019	42,000	39,500	34,200	40,200	40,300
1.827	39,900	37,400	32,700	41,500	35,400
1.653	33,000	35,300	31,400	39,700	34,100
1.496	31,600	33,100	30,000	38,800	32,500
1.353	30,300	30,700	28,900	37,200	30,600
1.225	29,100	28,600	28,500	34,800	28,300
1.108	26,000	27,300	27,900	33,200	32,880
1.003	20,700	26,200	27,100	30,600	24,500
0.9072	18,300	24,200	26,400	27,100	22,900
0.8208	17,400	23,300	25,600	26,700	28,800
0.7427	20,400	22,700	25,000	19,300	31,500
0.674	19,600	22,200	23,800	19,900	21,400
0.6081	15,300	21,300	22,500	19,900	25,000
0.5502	12,500	20,100	21,100	17,000	23,100
0.4979	13,900	18,800	19,700	13,700	22,300
0.4505	14,700	17,700	14,000	14,700	20,400
0.4076	16,600	16,800	11,900	16,200	24,300
0.3688	16,900	16,300	11,100	14,600	17,600
0.3337	9,740	15,300	10,400	14,800	14,400
0.3020	8,960	14,300	9,640	15,900	16,300
0.2752	7,980	13,300	8,970	15,700	17,800
0.2472	7,900	12,400	8,300	12,200	11,000
0.2237	7,720	11,600	7,700	13,400	11,800
0.2024	7,200	10,900	7,100	7,960	17,400
0.1832	9,580	10,200	6,570	12,300	12,000
0.1657	6,980	9,450	6,090	12,900	14,200

* Function is $E_d^{th} \times F(E)$. To obtain dpa per n/cm^2, multiply by $\frac{1}{(E_d)} \times 10^{-24}$ preferred

For these calculations $\frac{0.6 \times 10^{-24}}{E_d^{th}}$ is used.

Table 1 (continued)

Lower Energy MeV	316 SS	Mo	Nb	V	Al
0.1500	6,460	8,690	5,650	12,800	23,400
0.1357	8,890	7,940	5,230	7,900	17,300
0.1228	6,430	7,220	4,860	9,610	5,300
0.1111	3,590	6,520	4,510	12,700	7,300
0.08652	5,120	5,540	3,970	4,290	12,300
0.06738	5,880	4,360	3,190	7,040	5,800
0.05247	2,980	3,420	2,540	8,980	1,700
0.04087	2,840	2,700	2,030	3,022	2,600
0.03183	2,680	2,140	1,640	2,650	8,800
0.02479	7,600	942	1,310	3,620	9,700
0.01930	714	1,700	1,030	8,900	3,800
0.01503	1,200	1,350	836	11,300	4,400
0.01171	1,160	1,070	667	10,200	4,400
eV					
9119	756	838	546	2,710	3,400
7102	1,260	653	473	9,440	2,800
5531	810	513	383	5,860	4,200
4307	617	403	306	838	1,800
3355	452	318	245	676	1,400
2613	288	249	198	239	1,100
2035	203	231	160	141	840
1585	117	191	131	102	650
1234	127	160	109	60.8	500
961.1	230	136	91.1	34.9	380
748.5	78.4	120	77.6	19.1	290
582.9	63.2	134	73.3	10.3	220
457.3	48.1	107	79.4	10.2	160
353.6	5.03	118	79.4	12.3	120
275.4	5.07	91.0	79.4	14.9	85
214.5	5.70	51.2	79.4	6.58	59
167.0	6.35	66.0	79.4	10.9	38
130.1	7.17	144	79.4	25.4	23
101.3	8.10	126	79.4	21.3	13
78.89	9.10	94.0	79.4	10.1	15
61.44	10.2	190	79.4	11.1	21
47.65	11.54	584	79.4	12.9	25
37.27	13.1	945	79.4	14.4	29
29.02	14.8	184	79.4	16.8	32
22.60	16.8	26.2	79.4	19.4	26
17.60	19.1	12.4	46.5	21.5	35
13.71	21.6	19.1	2.50	24.2	37
10.68	24.6	39.3	2.83	27.4	38
8.315	27.6	20.8	3.22	31.2	44
6.476	31.2	12.3	3.64	35.2	62
5.043	35.3	11.8	4.13	39.9	77
3.928	40.0	12.5	4.67	45.2	89
3.059	45.4	13.9	5.29	50.8	98

Table 1 (continued)

Lower Energy eV	316 SS	Mo	Nb	V	Al
2.382	51.3	14.7	5.99	58.0	110
1.855	58.2	16.6	6.81	65.7	110
1.445	66.8	18.8	7.69	74.5	110
1.125	76.3	21.3	8.73	84.4	120
0.8764	84.4	24.2	9.91	95.6	130
0.6826	95.0	27.4	11.2	108	190
0.5316	108	31.0	12.7	123	240
0.4140	122	35.2	14.4	158	280
0.0220	212	61.0	24.9	273	390

D. Gas Production Cross Sections

The gas production cross sections for Nb, V, Al, oxygen, and 316 stainless steel were obtained from ENDF/B-III and averaged over the energy group structure used for the ANISN calculations by the MACK code[16]. Cross sections for molybdenum were calculated using Pearlstein's Model[31]. All the cross sections were assumed to be constant above 15 MeV for the LAMPF calculations following Dudziak[19]. No impurity (e.g. C,N,Si etc.) reactions were considered but the $^{58}Ni(n,\gamma)$ $^{59}Ni(n,\alpha)^{55}Fe$ reactions were considered in 316 SS. The cross sections of Kirouac[32] were used for the ^{59}Ni reactions. Figures 4a and 4b show how the (n,α) and (n,p) cross sections vary over the 0-15 MeV range. The curves in these figures do not include the (n,n'p), (n,d), (n,t) or $(n,n'\alpha)$ contributions but the calculated results reported later will include those contributions for SAP. The (n,n'p) cross sections will also be included for Ni and Cr.

III. Results

A. Displacement Rates

The calculated results for the five materials in the seven nuclear facilities considered here are given in Table 3. The displacement rates in the first wall of a fusion system vary from a low of 2.3×10^{-7} dpa/sec to 5.4×10^{-7} dpa/sec in Al. In all cases considered here, the fission reactors had higher displacement rates by a factor of 1.4 to 9.2 The two accelerator neutron sources considered have lower displacement rates than the first wall of the fusion blanket; LAMPF by a factor of ~3.4 and RTNS by a factor of 22. This latter number will always be a constant

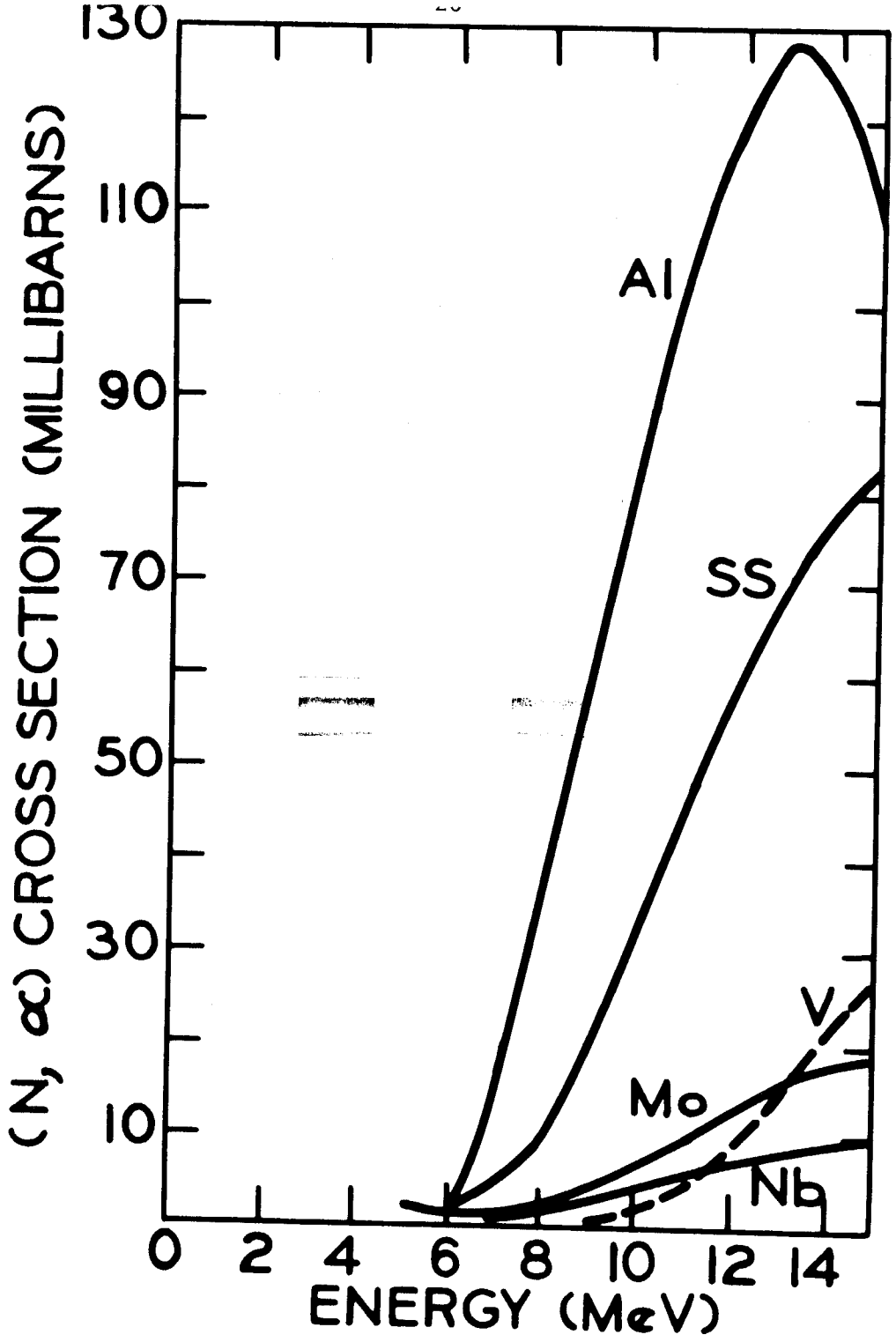

FIG. 4a. COMPARISON OF THRESHOLD (N, α) CROSS SECTIONS FOR 316 SS, V, Nb, Mo AND Al

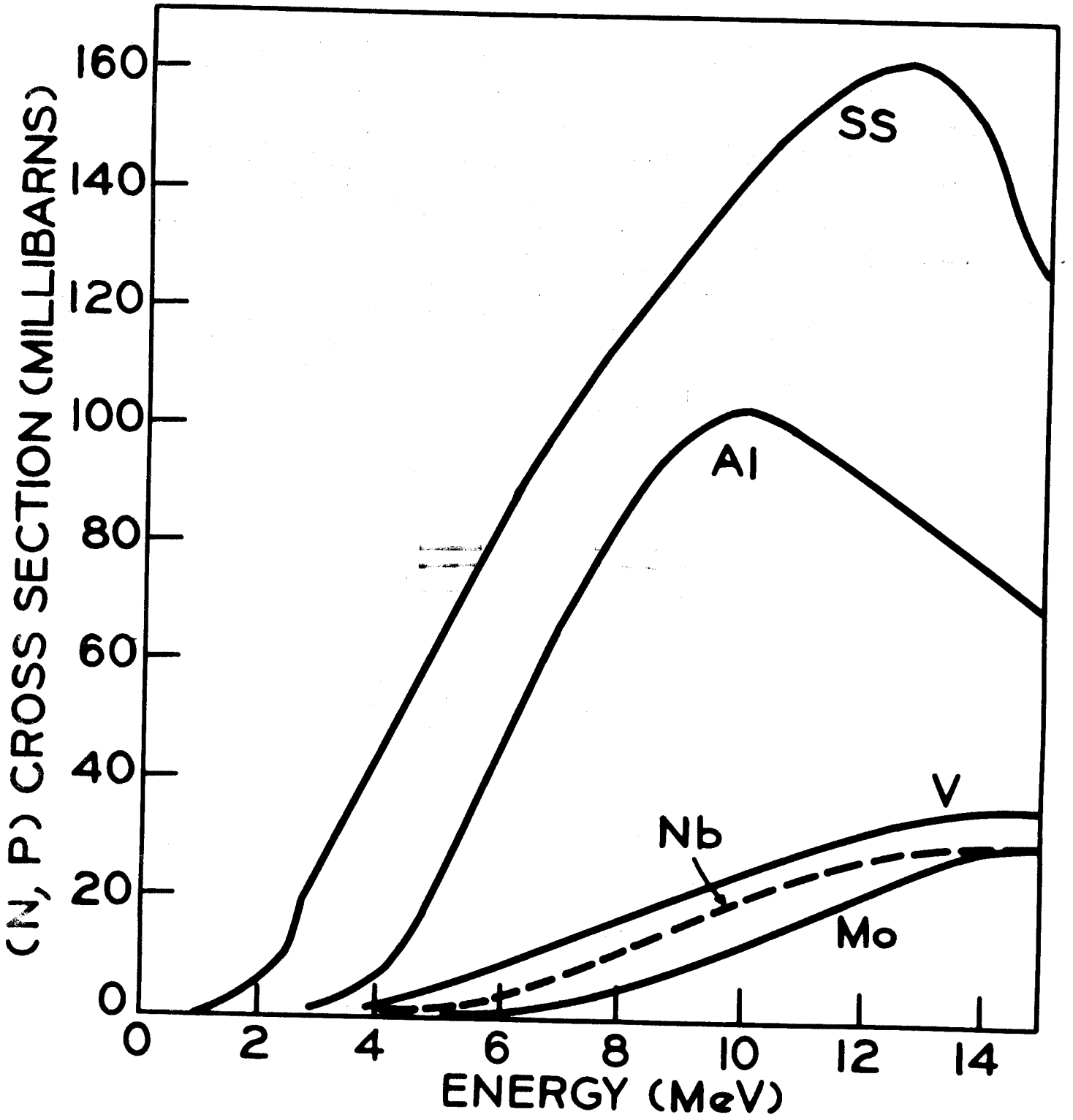

FIG. 4b. COMPARISON OF THRESHOLD (N, P) CROSS SECTIONS FOR 316 SS, V Nb, Al AND Mo

Table 3

Calculated Maximum Displacement Rates for
Typical Nuclear Facilities

Facility	dpa/sec x 10^7 316 SS	Nb	Mo	V	Al
Fusion Reactor (1 MW/m^2)	3.1	2.3	2.6	3.7	5.4
FFTF (400 MW)	26	16	19	34	49
EBR-II (62.5 MW)	14	9.0	9.6	17	24
HFIR (100 MW)	14	7.8	8.4	16	19
ETR (175 MW)	5.1	3.2	3.5	6.6	8.4
RTNS (2 x 10^{12} n $cm^{-2}sec^{-1}$, 14 MeV)	0.14	0.10	0.12	0.12	0.24
LAMPF (2 x 10^{14} n $cm^{-2}sec^{-1}$, Total)	0.84	0.6	0.6	1.1	1.4

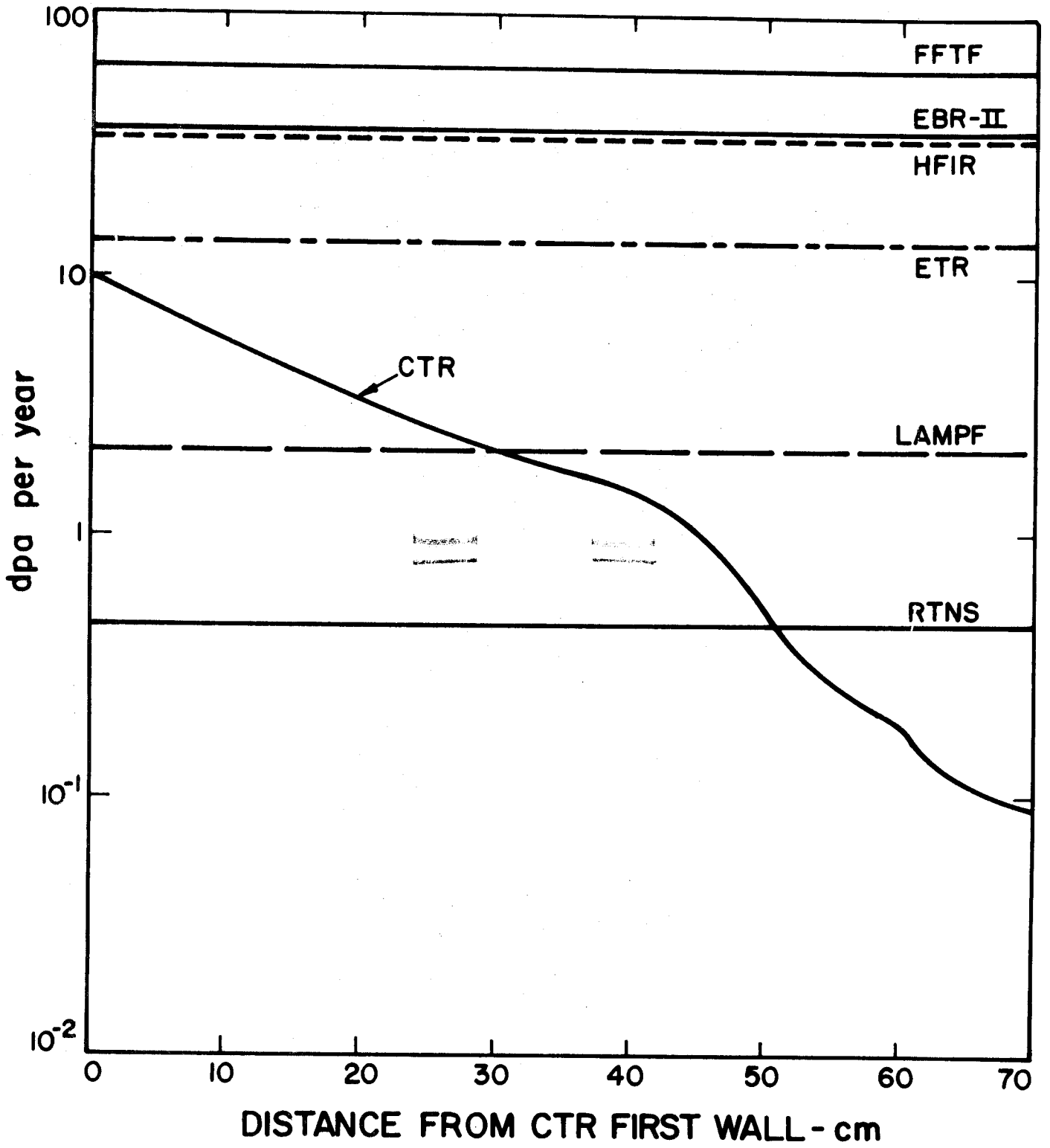

FIGURE 5 DISPLACEMENT RATE IN 316 STAINLESS STEEL FOR VARIOUS NUCLEAR FACILITIES ASSUMING A 100% PLANT FACTOR

factor of 22 below the fusion reactor numbers because of our previous assumption about the use of blankets on RTNS.

A comparison of the values in Table 3 to the variation of the damage in the CTR blanket composed of 316 SS is shown in Figure 5. It is noted again that in general the fission reactors can produce dpa rates greater than those found in a CTR blanket at a 1 MW/m^2 wall loading. On the other hand, the LAMPF and RTNS facilities can duplicate the displacement rates in only parts of the blanket that are >~40 cm or so from a moderately irradiated CTR first wall. The above remarks generally apply as well to the Mo, Nb, V and SAP systems.

B. Gas Production

The rate of helium and hydrogen generation in the materials of interest is listed in Table 4. Unlike the displacement calculations, there are dramatic differences between the gas production rates of the various materials in the same reactors. For example, the total helium production rate of SAP in the fusion system is twice that of 316 SS, over 7 times that in V and Mo and over 17 times that for Nb. A slightly different circumstance exists in fission facilities (e.g. HFIR) where the ^{59}Ni reactions cause over 100 times more helium to be formed in 316 SS than SAP. It is best at this point to discuss the results in terms of a specific gas in an individual material.

The calculated helium production in 316 SS ranges from a low of 1.5×10^{-7} appm per sec in EBR-II to 1330×10^{-7} appm per second after one year of irradiation in HFIR. The ETR facility produces close to the same amount of helium as does a fusion spectrum although the reactions in the two systems are completely different. In the thermal fission reactors (HFIR & ETR) most of the helium comes from the ^{59}Ni reaction whereas in the fast reactors most of the helium comes from primary reactions. It is important to remember

Table 4

Calculated Gas Production Rates for Typical Nuclear Facilities

Facility	Atomic parts per million per sec x 10^7					
	316 SS[a]	316 SS[b]	Nb	Mo	V	SAP
			Helium			
CTR	64	N	7.6	15	18	130
FFTF	2.5	N	0.53	0.95	0.15	5.5
EBR-II	1.5	N	0.31	0.57	0.097	2.5
HFIR	2.6	1330	0.57	1.0	0.15	5.8
ETR	0.61	48	0.15	0.27	0.030	1.3
RTNS	2.9	N	0.34	0.68	0.81	5.9
LAMPF	5.1	N	0.62	1.2	1.3	9.1
			Hydrogen Isotopes			
CTR	170		25	30	33	250
FFTF	133		3.6	1.8	7.7	33
EBR-II	85		2.1	1.1	4.6	16
HFIR	141		3.9	1.9	8.5	36
ETR	43		1.1	0.53	2.5	11
RTNS	7.7		1.1	1.4	1.5	11
LAMPF	19		2.23	2.5	2.8	19

(a) Primary reactions only

(b) Helium (in atomic parts per million per sec x 10^7) contribution from $^{58}Ni(n,\gamma)^{59}Ni(n,\alpha)$ after only one year of irradiation

N - negligible, $<<0.1 \times 10^{-7}$ appm sec^{-1}

that the rate of helium production is not constant in thermal fission reactors; it starts out constant but increases as $(\phi t)^2$ until such time as burn out in ^{59}Ni becomes important. Thereafter the production rate drops until it is eventually proportional to t to the first power again. The data in Table 3 is reported as the instantaneous rate from both helium threshold reactions and $^{59}Ni(n,\alpha)^{55}Fe$ reactions after one year of continuous operation.

Figure 6 shows an example of how the helium generation rates vary throughout a 316 SS CTR blanket. A comparison is also made to helium production in other facilities. It is noted that fast fission and accelerator sources considerably underproduce helium, by a factor of 10 or more, in steel compared to that in the first wall of a 1 MW/m^2 neutron irradiated CTR first wall. In fact, the non fusion sources cannot generate enough helium to duplicate the production rates in the first 40-50 cm of such a blanket. On the other hand, thermal reactors may duplicate the helium production rates up to ~7 MW/m^2.

The vanadium system has no thermal (n,α) reaction and therefore the amount of helium produced by the neutron facilities is only from primary reactions. The production rate in the CTR blanket is at least two orders of magnitude larger than that in fission reactors. It is interesting to note that the RTNS can produce helium at a rate 10 times that in the EBR-II and the helium production rate in the LAMPF facility is ~60% higher than that in the RTNS.

Niobium has the lowest helium production rate of any of the 5 materials considered here. However, the maximum value of 7.6×10^{-7} appm sec^{-1} in the fusion system is still more than a factor of 10 higher than for the best fission facilities. Another interesting point in this

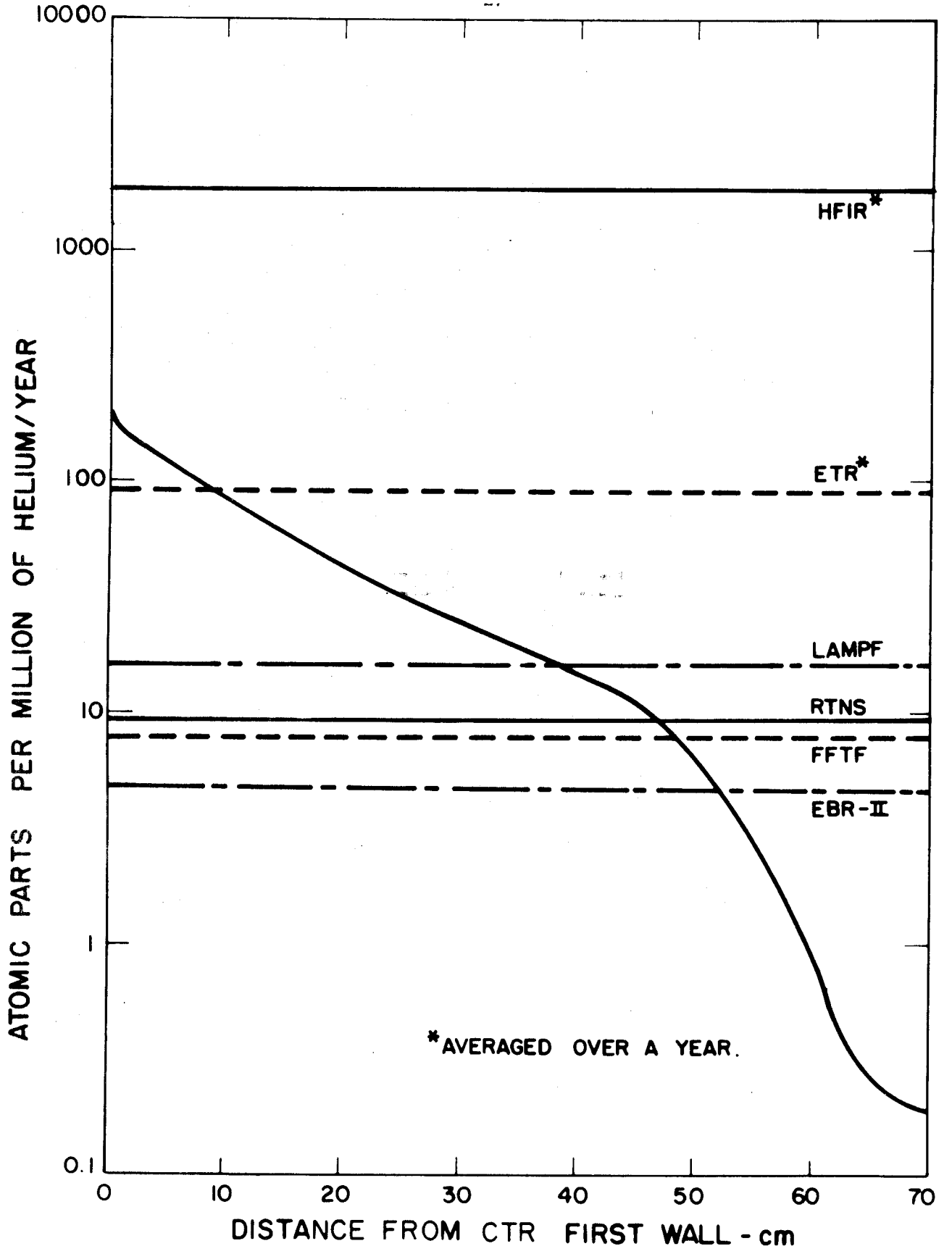

FIGURE 6 CALCULATED HELIUM PRODUCTION RATE IN 316 STAINLESS STEEL FOR VARIOUS NUCLEAR FACILITIES

metal is that the accelerator sources can produce helium in Nb at about the same rate as do the EBR-II and FFTF reactors.

The situation for Mo is slightly different than that of vanadium in that fission facilities and accelerator sources produce helium at a rate which is only one order of magnitude lower than in a fusion reactor.

The SAP alloy has the highest helium generation rates of any material considered here except for the steel in thermal fission reactors. About 10% of this high helium generation rate in the fusion reactor stems from the fact that the $(n,n'\alpha)$ reaction has been included in this calculation About 20% of the helium in SAP comes from (n,α) and $(n,n'\alpha)$ reactions in the oxygen of the Al_2O_3. However, even if the contribution from oxygen is subtracted, pure Al alone still produces more gas than any of the other materials considered here.

The major difference between the hydrogen isotope and helium production in 316 SS is that there is no thermal (n,p) cross section in steel and about 60% of the hydrogen in steel comes from nickel which is present as ~14 atomic percent. The hydrogen isotope production rates in SAP include a contribution from the aluminum (n,n'p) cross section of 12% and a 18% donation from the (n,d) reaction. Finally, it should be noted that while oxygen contributes ~20% of the helium to SAP, it only contributes 1% of the hydrogen isotopes.

Discussion

There are four main features of this work which deserve special discussion. They are

1. The similarity in the energy dependencies of the displacement cross sections for all the materials studied here.

2. The fact that displacement rates in all parts of CTR blankets

at moderate wall loading (~1 MW/m^2) are below those in current fission reactor research facilities (Figure 5).

3. The extremely high helium production rates for all materials in CTRs and for 316 SS in thermal reactors (Table 4 and Figure 7).

4. The large discrepancy between helium production rates in CTRs as opposed to most other research facilities (Table 4 and Figure 6).

The relative magnitudes of the displacement cross sections are uncertain to perhaps 30%. This is of minor importance in this work, however, because absolute comparisons of displacement rates of several materials in a given irradiation facility provide little or no information on comparative total damage rates. This is because of the extreme sensitivity of radiation damage to such variables as material purity and microstructure. Legitimate comparisons among materials of the spectrum dependence of the displacement rate can be made by first normalization all displacement rates in one spectrum to unity. When this is done, it is found that relative rates differ by $<\pm 25\%$ (generally considerably less). Hence, any conclusions made regarding the simulation of CTR displacement rates with fission reactors applies to all five of the materials studied.

It is interesting to note that even though we have calculated the displacement rate of solid members in a 4000 MW_{th} CTR, these rates are substantially below those which could be produced in lower power fission plants. This effect is mainly due to the size of CTRs and the substantial separation of the solid blanket members from the neutron generating media, (the plasma) in fusion systems. Figure 2 shows that, provided the wall loading of fusion systems doesn't exceed a few MW/m^2, all of the four fission reactors considered here can produce damage rates higher

Fig. 7

Helium Gas Production in 316 SS

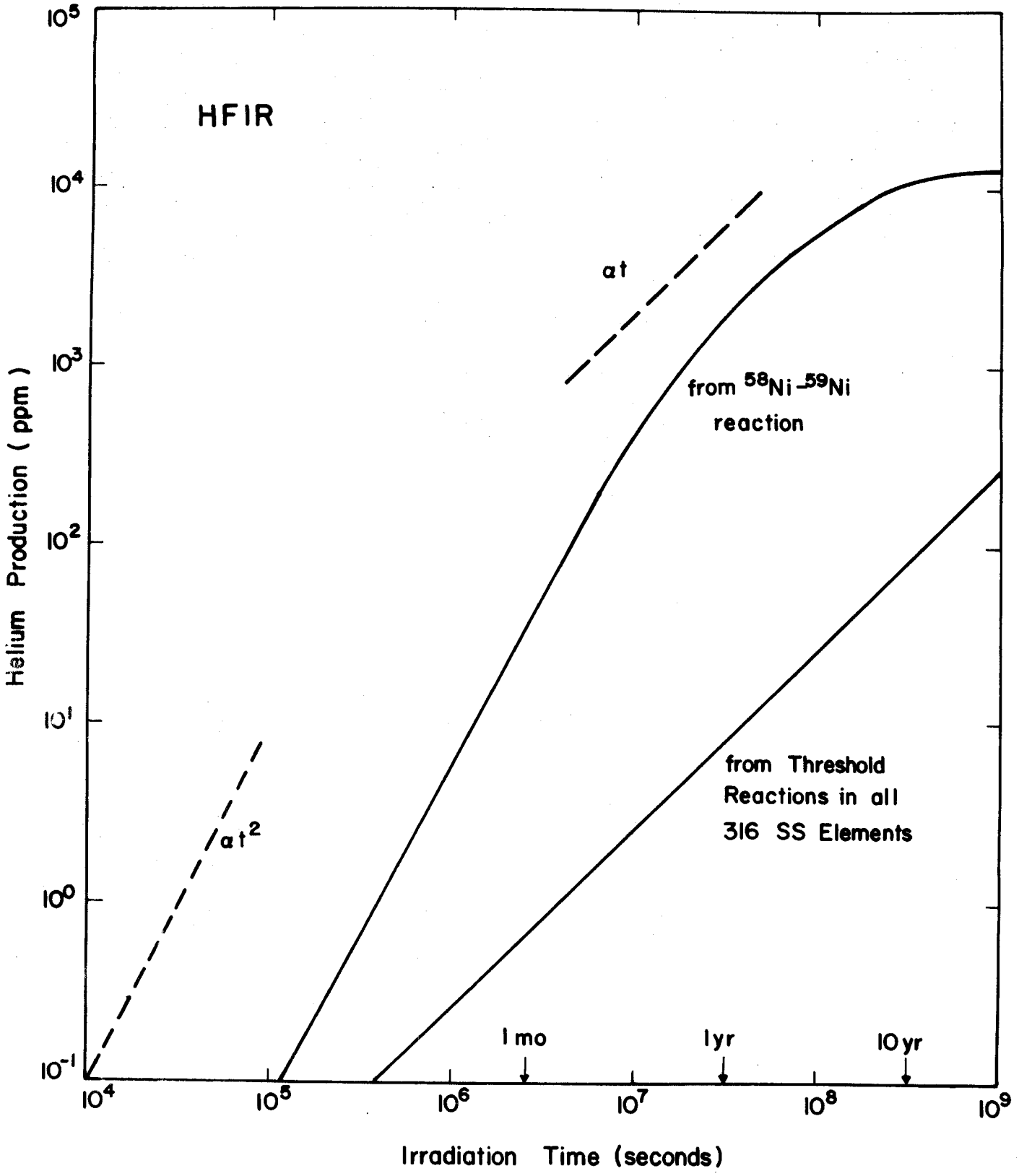

than in the CTR first wall. The FFTF can even duplicate displacement damage typical of ~7-9 MW/m^2 neutron wall loading.

An important point to note in Figures 5 & 6 is the fact that the total damage in the blanket could vary by more than 2 orders of magnitude. The variation in total damage for components which extend radially from the CTR first wall would introduce rather severe complications. Differential swelling, hardening or creep could cause local bending or warping of structural components and introduce unacceptable stresses. Not only could the total damage vary significantly but the damage rate could vary from as little as 3×10^{-9} dpa sec^{-1} at the outer edge of the blanket to ~3×10^{-7} dpa sec^{-1} at the first wall of a 1 MW/m^2 loaded system. Future irradiation programs will have to take both of these effects into account because recent evidence[33] has shown that at relatively moderate temperatures (30-50% of the melting point) the rate at which damage is induced may affect the final configuration of defects. It is also well known that such processes as creep, a higher temperature phenomenon, are also very sensitive to damage rate.[34]

Unlike the displacement results which are relatively insensitive to the material, the production of He or H in potential CTR materials depends very much on the elements considered. For example it can be seen that in the first wall of a CTR blanket the helium production rate in SAP is 7 to 17 times that of refractory metals while the displacement rates of these metals are within 25%. The hydrogen production rate in the SAP is also 4-5 times higher than for refractory metals. Because of the various threshold energies, the ratios are even more pronounced in fast fission facilities. Another good example is the helium production in steel in fast reactors. It occurs at a rate 5 times higher in 316 SS than in Nb and almost 3 times higher than in Mo. Hydrogen production in steel is 17 times higher than in V and 37 times higher than in Nb for fast reactors. On the other hand, thermal reactors like HFIR can produce helium in steel

more than 20 times faster than in fusion reactors if enough time is given for a buildup of ^{59}Ni. The buildup of He in 316 SS irradiated in in HFIR is shown in Figure 4. Initially (~<1 month) the helium production rate due to ^{59}Ni (n,α) reactions is proportional to t^2. After a few months, the production rate is proportional to the first power of time because the ^{59}Ni (n,γ) reaction begins to compete. Finally, when all of the ^{58}Ni atoms have been transmitted, there is no more helium produced by this type of reaction and only the high energy (n,α) reactions can contribute more helium. This complex behavior tends to emphasize the point that when scientists study irradiation induced phenomena which may be affected by gas atoms, (e.g. voids and ductility reductions) they must analyze the neutron spectra very carefully.

Variations of gas production in diffferent structural materials has certainly been expected by investigators. However, variations in gas production in the same material irradiated in different neutron spectra can also be important. Figure 3 shows that the absolute helium production rates in neutron test facilities could vary in stainless steel by two to three orders of magnitude. This is particularly important because the CTR blanket design considered here has a relatively low neutron wall loading (1 MW/m^2) and other sysyems have been designed to as high as 6 MW/m^2. [35] It is obvious from Figure 3 that even the FFTF, the highest flux fast reactor in the U.S., cannot duplicate much more than a 0.04 MW/m^2 wall loading from the standpoint of helium gas production but the ETR can duplicate a 0.75 MW/m^2 value and HFIR can duplicate the helium production rate of ~7 MW/m^2 wall loading. The high energy neutron facilities are within an order of magnitude of reasonable CTR gas generation.

The situation is somewhat worse for the refractory metals such as V where wall loadings of only ~0.01 MW/m^2 can be duplicated in FFTF and HFIR for the production of helium. The accelerator sources can duplicate helium production

rates of only 0.05 MW/m^2. The same conclusion applies to the other CTR metals and it is clear that no existing facility can duplicate the proper CTR gas production rates for Nb, V, Mo or SAP.

The previous points can be put into a little better perspective by calculating the ratio of the gas production to the displacement rates. The results are in Table 5 and Figures 8 and 9 display these values in a graphic manner. It is important to note that this ratio is not dependent on absolute flux values (with the exception of 316 SS) but depends only on energy spectra. Whereas, the appm He/dpa ratio in steel is ~20 in the CTR first wall, it is only 0.10 to 0.14 in fast fission reactors, but ~ 50 in HFIR after one year of irradiation. This ratio drops to ~ 6 in LAMPF. The ratio for V varies by ~ 3 orders of magnitude from CTRs to fast fission plants and it varies by ~2 orders of magnitude for SAP Mo in the same facilities. The high energy accelerator neutron facilities tend to have better ratios for the non-steel materials but they are still a factor of 3 or more lower than typical CTR values. Hence, any experiments done on non-CTR facilities which purport to correlate with CTR conditions must be closely examined in view of the He/dpa ratio.

The situation with respect to the H/dpa ratio is much the same as for the helium ratio as shown in Figure 8. This ratio varies by a factor of ~10 for steel when comparing such facilities as FFTF and the first wall of a CTR. There is also a one to two order of magnitude difference in the H/dpa ratio for Nb the same facilities.

One final point to notice from Figures 5-9 is that the HFIR reactor represents perhaps the best combination of dpa rates, He/dpa and H/dpa ratios for the materials considered here. The high flux FFTF has adequate dpa rates but H/dpa and He/dpa ratios which are quite low. Accelerator neutron sources produce close to the proper gas-displacement ratios but the absolute magnitude of the damage rate is so low that it could take ~10 years of irradiation to reproduce ~1 year of CTR first wall damage

Table 5

Calculated Maximum Gas Production to dpa Ratios for Typical Nuclear Facilities

	appm He/dpa					appm H/dpa				
Facility	316 SS	Nb	Mo	V	SAP	316 SS	Nb	Mo	V	Al
CTR	20	3.4	6	4.7		54	11	12	8.8	46
FFTF	0.10	0.033	0.050	0.0043	0.11	5.0	0.22	0.10	0.23	0.68
EBR-II	0.11	0.035	0.060	0.0058	0.11	6.2	0.23	0.11	0.26	0.67
HFIR	50*	0.074	0.12	0.010	0.30	10	0.5	0.23	0.55	1.8
ETR	3.8*	0.028	0.08	0.0045	0.16	8	0.34	0.15	0.38	1.3
RTNS	20	3.4	6	4.7	24	54	11	12	8.8	46
LAMPF	6.0	1.0	1.7	1.2	6.3	23	3.8	4.2	2.6	13

*Average over the year

FIGURE 8. CALCULATED HELIUM TO DISPLACEMENT RATIO IN VARIOUS NUCLEAR FACILITIES

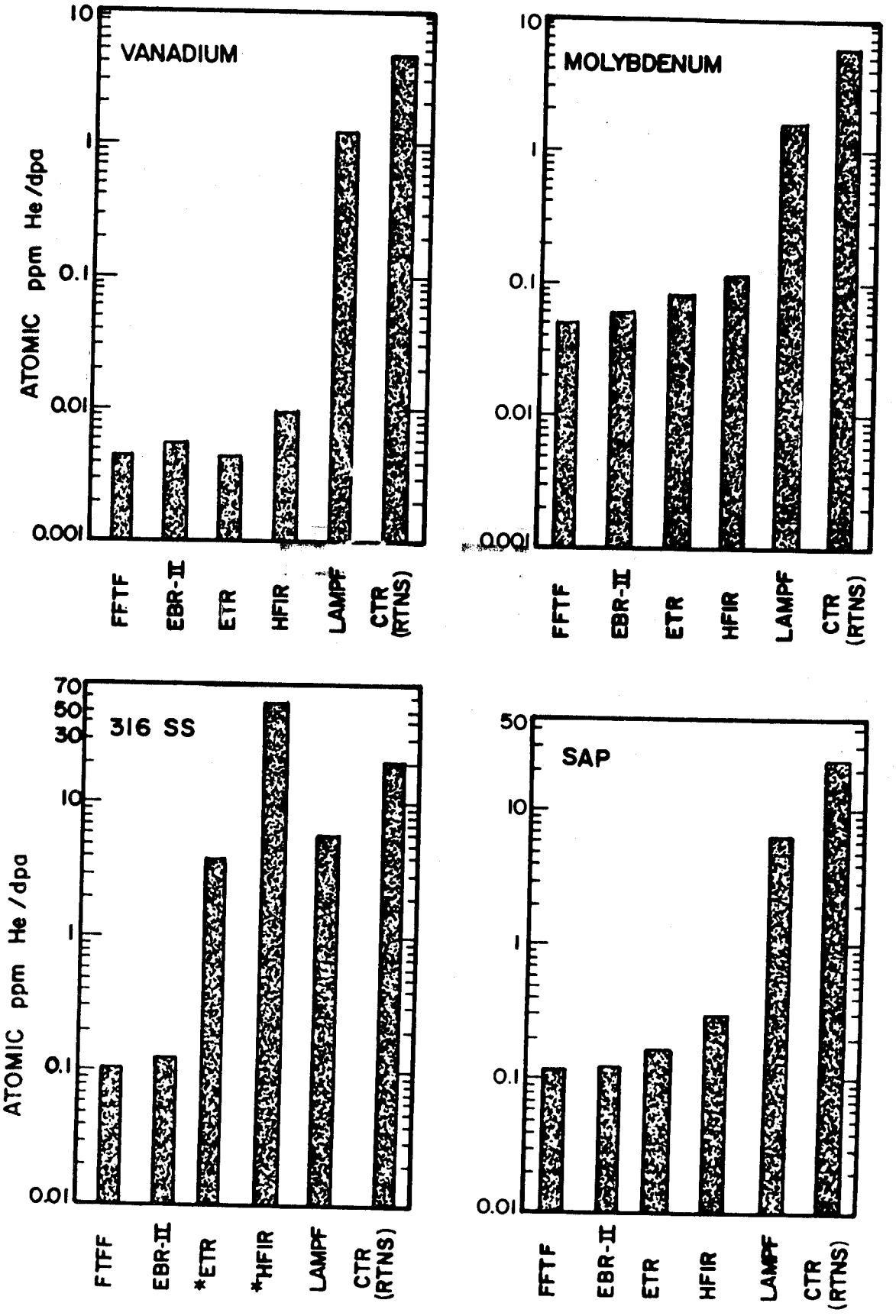

*AVERAGE OVER ONE YEAR

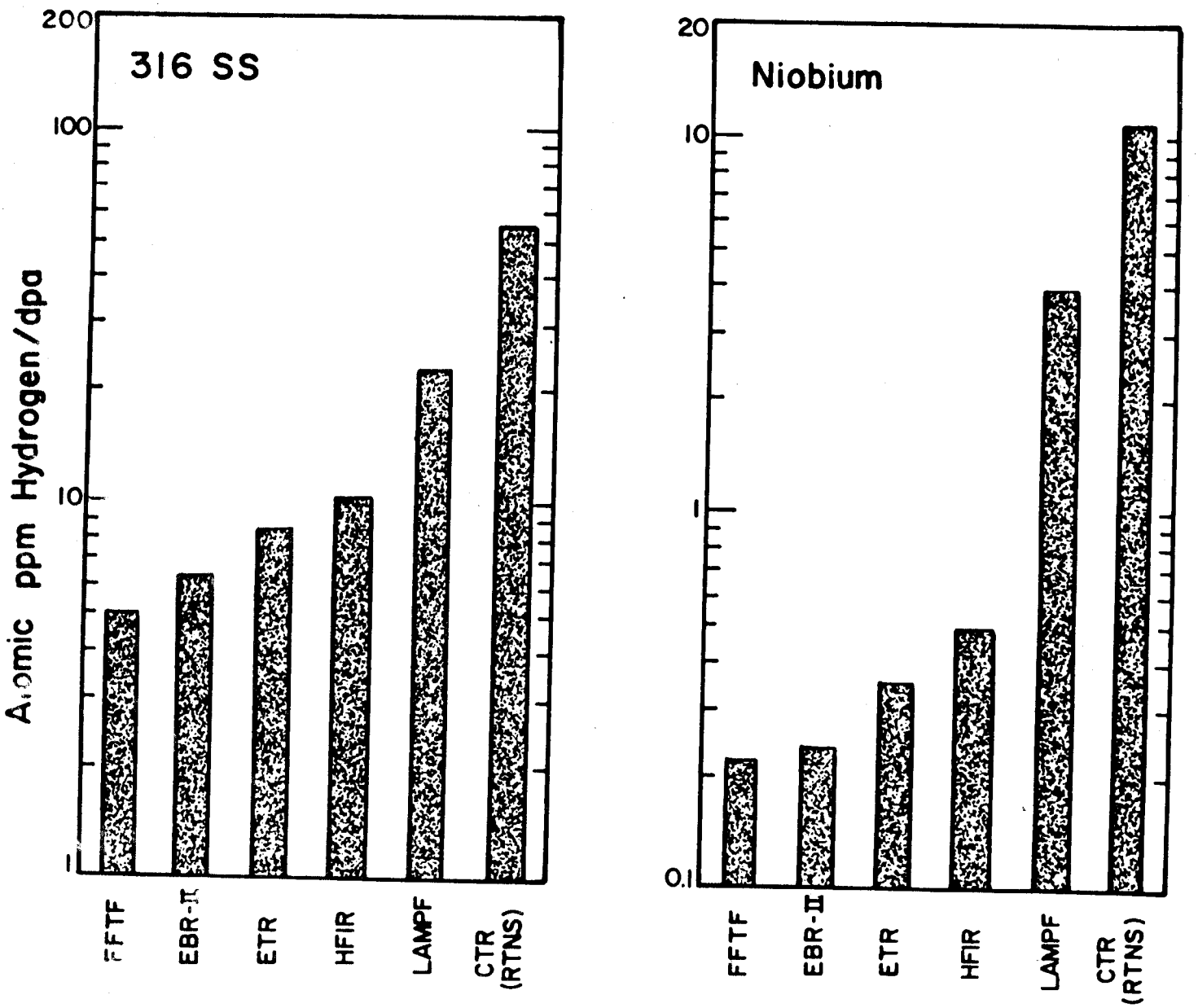

FIGURE 9. CALCULATED HYDROGEN TO DISPLACEMENT RATIO IN 316 SS AND NIOBIUM

due to gas effects. Improvement in these facilities by a factor of ten would make them much more attractive as irradiation test facilities.

V. Conclusions

- The variation of the spectrum averaged displacement cross section among existing irradiation facilities is the same, to within ±25%, for Nb, Mo, V, Al, and 316 SS.
- There will be large variations in the rate at which atoms are displaced in a standard CTR blanket, up to a factor of 100 in this study.
- Several present neutron facilities can duplicate displacement rates in CTR blankets with ~ 2-8 MW/m^2 neutron wall loadings.
- The relative helium production rates in the first wall of a CTR blanket will vary in the following proportion for SAP, 316 stainless steel, V, Mo or Nb; 17/8.4/2.4/2/1. Similar numbers for hydrogen generation vary in the ratio of 10/6.8/1.3/1.2/1.
- The helium production rates in the first wall of a CTR in appm per year per MW m^{-2} wall loading are 410/202/57/47/24 for SAP, 316 SS, V, Mo and Nb, respectively. Similar numbers for hydrogen are 790/540/100/95/79.
- The variation in helium production rates from the first wall of a standard CTR to the outer edge of the blanket is ~1000.
- While there are large variations from element to element, it is clear that fast fission reactors will produce appm helium/dpa ratios which are a factor of ~100 or lower than that produced in the first wall of CTR blankets.

- The helium production rates in 316 SS in thermal fission reactors can be even higher than in fusion reactor blankets due to the buildup of ^{59}Ni and the subsequent (n,α) reactions. Helium production rates of several thousand atomic ppm per year can be achieved in high flux thermal reactors like HFIR.
- All current fission reactors will produce a appm hydrogen/dpa ratio of 5 to100 times lower than that found in the first wall of CTR blankets.
- High energy neutron sources such as the RTNS and LAMPF facility can produce gas/dpa ratios close to, or within a factor of 4, those found in CTR blankets. However, the absolute magnitude of gas production is lower by a factor of 10 or more.
- The thermal reactor HFIR appears to have the best combination of displacement and gas production rates and gas/displacement ratios with which to conduct present CTR materials studies, especially for stainless steel.

Acknowledgement

The authors would like to thank the Wisconsin Electric Utilities Research Foundation and the U.S.A.E.C. Controlled Thermonuclear Research Division, and the U.S.A.E.C. Reactor Research and Development Division for their support of this work. We would also like to thank Dr. Donald Dudziak for allowing us to use LAMPF spectra.

References

1. "Nuclear Fusion Reactors," Proceedings of the British Nuclear Energy Society Conference held at Culham Laboratory, Sept. 1969.

2. Steiner, D., Nucl. Appl. Tech., Vol. 9, 1970, p. 83.

3. See the proceedings of the International Working Sessions on "Fusion Reactor Technology" held at Oak Ridge, Tenn., June 28, 1971. CONF-710624.

4. See the proceedings of the meeting on "Fusion Reactor First Wall Materials" held at Germantown, Md., January 1972. WASH-1206.

5. Kulcinski, G. L., Brown, R. G., Lott, R. G., and Sanger, P. A., Nucl. Tech., Vol. 22, 1974, p.11.

6. See the proceedings of the International Conference on "Radiation Induced Voids in Metals" held at Albany, New York, June 9, 1971 and edited by J. W. Corbett and L. C. Ianniello.

7. "Voids Formed by Irradiation of Reactor Materials," British Nuclear Energy Society, Reading, England, 1971.

8. See "Effects of Radiation on Substructure and Mechanical Properties of Metals and Alloys, ASTM STP 529, American Society for Testing and Materials, 1973.

9. Holmes, J. J., Lovell, A. J., and Fish, R. L., ibid, p. 383.

10. Bloom, E. E., p. 93 in "Irradiation Embrittlement and Creep in Fuel Cladding and Core Components," BNES, London, 1973.

11. Kramer, D., Garr, K. R., Pard, A. G., and Rhodes, C. G., ibid, p. 109.

12. Hirsch, R. L., "Proceedings of the 1972 International Conference on Nuclear Solutions to World Energy Problems," American Nuclear Society, Hinsdale, Illinois, 1973, p. 216.

13. Badger, B., Abdou, M. A., Boom, R. W., Brown, R. G., Cheng, T. E., Conn, R. W., Donhowe, J. M., El-Guebaly, L. A., Emmert, G. A., Hopkins, G. R., Houlberg, W. A., Johnson, A. B., Kamperschroer, J. H., Klein, D., Kulcinski, G. L., Lott, R. G., McAlees, D. G., Maynard, C. W., Mense, A. T., Neil, G. R., Norman, E., Sanger, P. A., Stewart, W. E., Sung, T., Sviatoslavsky, I., Sze, D. K., Vogelsang, W. F., Wittenberg, L., Yang, T. F., Young, W. D., UWFDM-68, Vol. I, November 1973.

14. Engle, W. W., "A Users Manual for ANISN. A One Dimensional Discrete Ordinated Transport Code with Anisotropic Scattering," USAEC Report K-1693, 1967.

15. M. K. Drake, Editor, "Data Formats and Procedures for the ENDF Neutron Cross Section Library," BNL-50279 (Oct. 1970).

16. Abdou, M. A., Maynard, C. W., and Wright, R. Q., ORNL-TM-39994, 1973.

17. Powell, J. R., Miles, F. T., Aronson, A., and Winsche, W. E., BNL-18236, June 1973.

18. Kam, F. B. K., and Swanke, J. H., ORNL-TM-3322, March 1971.

19. Dudziak, D. J. and Sherman, M. A., LA-DC-72-1364, 1972 and unpublished results.

20. Booth, R., and Barschall, H. H., Nucl. Inst. Meth., Voll. 99, 1972, p.1.

21. Lindhard, J., Nielsen, V., Schraff, M., and Thomsen, P. V., Mat, Fys. Medd. Dan. Vid. Selsk, Vol. 33, No. 10, 1963.

22. Robinson, M. T., "Nuclear Fusion Reactors," proceedings of the British Nuclear Energy Society Conference held at Culham Laboratory, Sept. 1969, p. 364.

23. Doran, D. G., Beeler, J. R. Dudey, N. D, and Fluss, M. J., HEDL-TME-73-76, December 1973.

24. Youngblood, G., Myhra, S., and DeFord, J. W., Coo-1494-7, 1968.

25. Lucasson, P. G. and Walker, R. M., Phys. Rev., Vol. 127, 1962, p. 485.

26. Neely, H. M., and Bauer, W., Phys. Rev., Vol. 149, 1966, p. 535.

27. Doran, D. G., Nucl. Sci. Engr., Vol. 49, 1972, p. 130.

28. Orphan, V. J., Rasmussen, N. C., and Harper, T. L., Gulf Atomic Report, GA-10248, July 1970.

29. Odette, G. R., private communication.

30. Segev, M., ANL-7710, January 1971.

31. Pearlstein, S., Journal of Nuclear Energy 27, 81 (1973).

32. Kirouac, G., unpublished results.

33. Sprague, J. A. and Smidt, F. A. Jr., Naval Research Laboratory Report, NRL-2629, August 1973, p. 27.

34. Harkness, S. D., Yaggee, F. L., and Styles, J. W., Argonne National Laboratory Report, ANL-7783, 1971, p. 68.

35. Thomassen, K. I. and Krakowski, R. A., Los Alamos Scientific Laboratory Report, LA-UR-73-1365, Sept. 1973.